Improving GRAPPA reconstruction by frequency discrimination in the ACS lines[1]

Santiago Aja-Fernández

LPI, ETSI Telecomunicación, Universidad de Valladolid, Spain

Email: sanaja@tel.uva.es

Gonzalo Vegas-Sánchez-Ferrero

LPI, ETSI Telecomunicación, Universidad de Valladolid, Spain

Email: gvegsan@lpi.tel.uva.es

Antonio Tristán-Vega

LPI, ETSI Telecomunicación, Universidad de Valladolid, Spain

Email: atriveg@lpi.tel.uva.es

Abstract

GRAPPA is a well know parallel imaging method that recovers the MR magnitude image from aliasing by using a weighted interpolation of the data in **k**-space. To estimate the optimal reconstruction weights, GRAPPA uses a band along the center of the **k**-space where the signal is sampled at the Nyquist rate, the so-called Autocalibrated (ACS) lines. However, while the subsampled lines usually belong to the medium-high frequency areas of the spectrum, the ACS lines include the low frequency areas around the DC component. The use for estimation and reconstruction of areas of the **k**-space with very different features may negatively affect the final reconstruction quality. We propose a simple, yet powerful method to eliminate this artifact, based on the discrimination of the low frequency spectrum. We empirically show this approach achieves great enhancement rates, while keeping the same complexity of the original GRAPPA.

Key words: GRAPPA, parallel imaging, estimation

INTRODUCTION

The GeneRalized Autocalibrated Partially Parallel Acquisitions (GRAPPA) (1) is one of the most prominent Parallel Imaging reconstruction techniques for subsampled multiple-coil MR data. The reconstruction takes place into the **k**-space, where the missing lines are interpolated by a weighted combination of the adjacent acquired lines. The weights used in the reconstruction are estimated from the acquired data themselves by solving an overdetermined system of linear equations posed over the so-called Autocalibrated (ACS) lines. The ACS lines are a set of lines from the center of the **k**-space which are sampled at the Nyquist rate (i.e., unaccelerated). As shown in Fig. 1-left, the ACS lines involve the center of the **k**-space (low frequencies of the image) as well as the high frequency areas. Since the subsampled areas of the **k**-space are usually in the medium to large frequencies, the inclusion of the DC and low frequency components in the estimation may bias the reconstruction weights.

In order to improve the reconstruction performance of GRAPPA, many authors have proposed modifications to the original algorithm. Most of the efforts have been oriented to the reconstruction step rather than the estimation of the interpolation weights, like using self-calibrating iterative methods (2), banks of filters (3), (4)), image support reduction via a high-pass filtering (5), or kernel-based approaches (nonlinear GRAPPA) (6). However, some authors did detect the problem of estimation and proper selection of the ACS lines. In (7) the authors propose a different sampling pattern of the ACS, and in (8) a method to remove outliers before estimating the weights is suggested instead.

In this paper, we propose a simple but effective method to estimate the GRAPPA weights that highly improves the final quality of the reconstructed image. It is based on the removal of the low frequency areas of the ACS lines only during the estimation step, to avoid the bias they introduce in the reconstruction weights. The method is fully compatible with the original GRAPPA formulation, and it can be easily implemented into the commercial scanning software. In addition, the method is also compatible with other optimization methods proposed in literature.

THEORY

Estimation of the GRAPPA reconstruction weights

The original GRAPPA reconstruction strategy estimates the full **k**-space in each coil from a sub–sampled **k**-space (1), (9), (10) acquisition. While the sampled data $s_l^{\mathcal{S}}(\mathbf{k})$ remains the same, the reconstructed lines $s_l^{\mathcal{R}}(\mathbf{k})$ are estimated through a linear combination of the existing samples. Weighted data in a neighborhood $\eta(\mathbf{k})$ around the estimated pixel from several coils is used for such estimation:

$$s_l^{\mathcal{R}}(\mathbf{k}) = \sum_{m=1}^{L} \sum_{\mathbf{c} \in \eta(\mathbf{k})} s_m^{\mathcal{S}}(\mathbf{k} - \mathbf{c}) \omega_m(l, \mathbf{c}), \qquad [1]$$
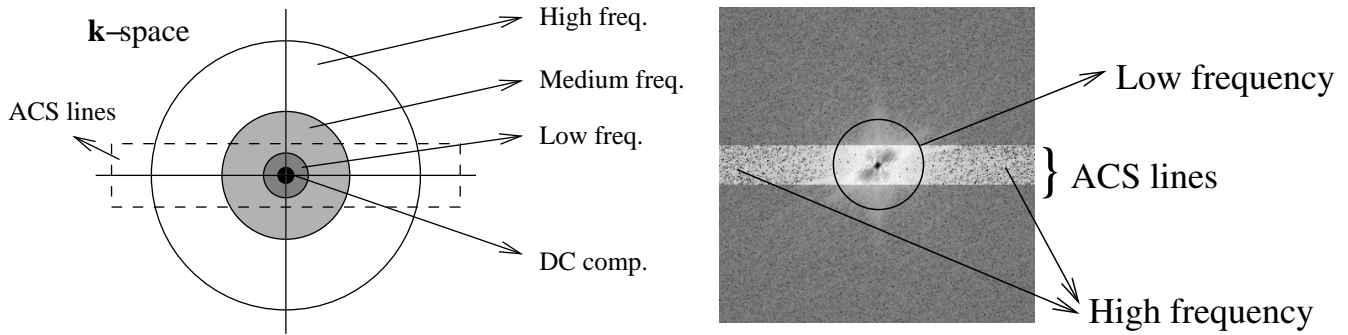
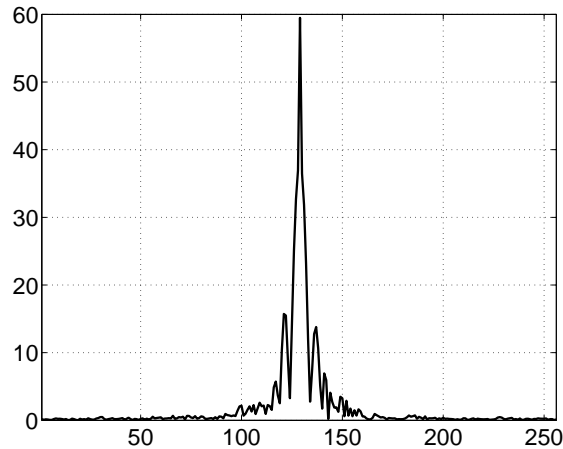**Figure 1.** Frequency distribution in the **k**-space of 1 coil.

Figure 2. Average of the magnitude of the 32 ACS lines of a 8-coil acquisition (**k**-space).

with $s_l(\mathbf{k})$ the complex signal from coil l at point $\mathbf{k}$ and $\omega_m(l, \mathbf{k})$ the complex reconstruction coefficients for coil l. These coefficients are determined from the center lines of the **k**-space, the so-called ACS lines, which are sampled at the Nyquist rate (i.e. unaccelerated) as shown in Fig. 1. The weights $\omega_m(l, \mathbf{k})$ are obtained using eq. ([1]) over these ACS lines

$$s_l^{\text{ACS}}(\mathbf{k}) = \sum_{m=1}^{L} \sum_{\mathbf{c} \in \eta(\mathbf{k})} s_m^{\text{ACS}}(\mathbf{k} - \mathbf{c})\omega_m(l, \mathbf{c}), \ \ l = 1, \cdots, L \qquad [2]$$

and fitting the resultant equation with some optimization method.

Frequency discrimination of the ACS components

Since the estimated weights are the same for each point within the image for every coil (they do not depend on **k**), there is a major problem with the estimation: while the subsampled lines usually belong to the medium-high frequency areas of the spectrum, the ACS lines include the low frequency areas around the DC component (see Fig. 1 for illustration). The use for estimation and reconstruction of areas of the **k**-space with very different features may negatively affect the final reconstruction quality.

The influence of the different areas of the spectrum over the final image is a very well-know topic in the signal processing field (11). However, in GRAPPA, the different properties of the spectrum are not taken into account when estimating the reconstruction weights. As a result, there is a bias due to the low frequency components in the final coefficients that worsens the reconstruction.

As an illustration, in Fig. 2, the average of the magnitude of the 32 ACS lines of a 8-coil acquisition is depicted. Note that, clearly, the signal around the DC component has very different properties in shape and magnitude when compared to the medium and high frequency areas.

Accordingly, the center of the **k**-space will have most of the energy of the ACS components. In Fig. 3 the ratio between the energy of a centered square window of size $N \times N$ with the total ACS energy is depicted for data sets 1 and 2 (later explained in section III). Note that a 5×5 window represents the 80% of the energy of the ACS lines, while a 31×31 window has more than 95% of the energy.

Our proposal to improve the estimation of the weights lays on a proper selection of the coefficients within the ACS lines, which advises discarding of those points around the DC component. Although more developed approaches can be made, in this work we
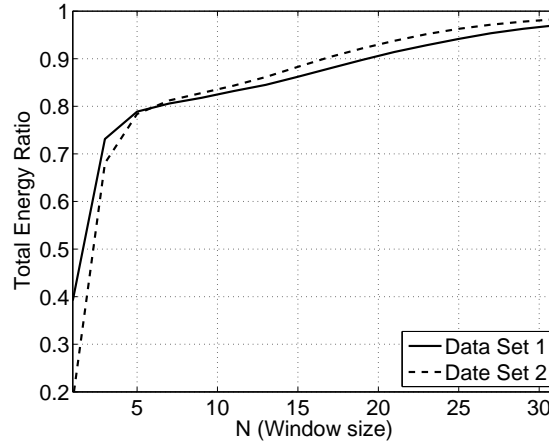
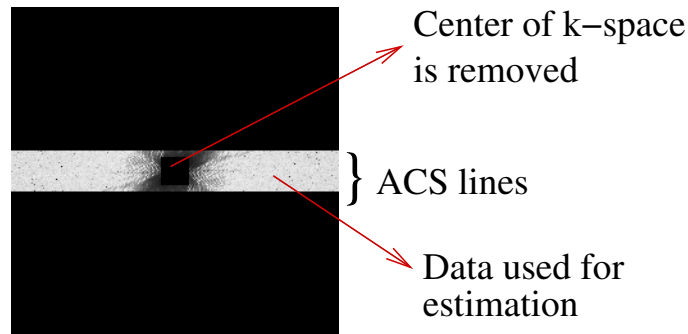**Figure 3.** Ratio of the energy of a square window centered in the DC component as a function of the size.

Figure 4. New estimation area ACS$_\mathcal{R}$

simply propose the elimination of a square window in the center of the **k**-space, as shown in Fig. II-B. Thus, the data used for estimation will be a subset of the ACS lines:

$$\text{ACS}_\mathcal{R} = \text{ACS} - \{\mathcal{C}_\mathbf{k}[N \times N]\}$$

where ACS stands for all ACS points, and $\mathcal{C}_\mathbf{k}[N \times N]$ is a $N \times N$ square centered in the DC component. Other shapes may be used; a square was elected for the sake of simplicity.

If we assume a symmetrical distribution of the energies of the frequency components around the center of the **k**-space, the removed window will accomplish all the center of the ACS, leaving some lines in the top and the bottom available for reconstruction. The number of lines will depend on the acceleration rate, R. Thus, for a symmetrical distribution of the energies, we can define the optimal size of N as

$$N_\text{opt} = |\text{ACS}| - (R+1) \tag{3}$$

where $|\text{ACS}|$ is the number of ACS lines. However, in practical situations, the energy distribution is not totally symmetrical and therefore it is advisable to choose a smaller window:

$$N \leq |\text{ACS}| - (R+1).$$

The assumption in eq. [3] will later be tested on the experiments section.

The method proposed is totally compatible with the existing GRAPPA, and can be easily included in the scanner software. The reduction of the amount of data used for estimation goes along with a reduction on the number of equations to fit in eq. ([2]), and, in some cases, that also means an acceleration of the estimation.

As a final recall, note that the center of the **k**-space is acquired, and although it is not used for coefficient estimation, it is indeed used for reconstruction. Such a simple approach will highly improve the reconstruction, as shown in the following experiments.

MATERIALS AND METHODS

For numerical validation of the method, three non accelerated acquisitions are considered:

- Data set 1 (DS1): an 8-channel head coil data acquired on a GE Signa 1.5T EXCITE scanner, FGRE Pulse Sequence, TR/TE=500/13.8, matrix size 256×256, FOV=20×20cm.

| Window Size | Square Window | | | | Round Window | | | |
| | Data Set 1 | | Data Set 2 | | Data Set 1 | | Data Set 2 | |
	MSE	SSIM	MSE	SSIM	MSE	SSIM	MSE	SSIM
0	3.5086	0.9012	5.8274	0.8096	3.5086	0.9012	5.8274	0.8096
1	3.3022	0.9110	5.5239	0.8227	3.5489	0.8997	5.8738	0.8073
3	3.1600	0.9173	4.9119	0.8486	3.2367	0.9140	5.3516	0.8303
5	2.8816	0.9291	4.4455	0.8700	3.0903	0.9204	4.9279	0.8484
7	2.5768	0.9419	4.0476	0.8903	2.8268	0.9317	4.4411	0.8705
9	2.4586	0.9470	3.9116	0.8975	2.6143	0.9406	4.0975	0.8874
11	2.4338	0.9483	3.8009	0.9025	2.4857	0.9460	3.9542	0.8952
13	2.3249	0.9524	3.6841	0.9080	2.4367	0.9481	3.8253	0.9015
15	2.2222	0.9563	3.5622	0.9137	2.3278	0.9523	3.7399	0.9056
17	2.1760	0.9581	3.4867	0.9170	2.2557	0.9550	3.6230	0.9109
19	2.1466	0.9592	3.4255	0.9199	2.2003	0.9572	3.5348	0.9150
21	2.1118	0.9605	3.3594	0.9230	2.1663	0.9585	3.4875	0.9172
23	2.0611	0.9624	3.3061	0.9254	2.1422	0.9594	3.4232	0.9202
25	2.0321	0.9636	3.2245	0.9294	2.1133	0.9605	3.3719	0.9228
27	1.9927	0.9654	3.1226	0.9344	2.0764	0.9619	3.3018	0.9262
29	**1.9670**	**0.9674**	**3.0829**	**0.9373**	2.0430	0.9633	3.2340	0.9299
31	2.1773	0.9663	3.2919	0.9362	2.0077	0.9650	3.1677	0.9338

TABLE I. Reconstruction performance for different size N of the Removed Window $\mathcal{C}_{\mathbf{k}}[N \times N]$ for the 3 Data Sets, acceleration factor $R = 3$ and 32 ACS lines. Square and round windows are considered.

- Data set 2 (DS2): MR data-set from (12) (the authors provide their data on-line[1]); eight-channel head array from 3 Tesla GE scanner, FGRE sequence, TR/TE=300/10, matrix size 256×256, FOV=22×22cm.
- Data set 3 (DS3): a dopped ball phantom, scanned in an 8-channel head coil on a GE Signa 1.5T EXCITE 12m4 scanner with FGRE Pulse Sequence, matrix size 128×128, TR/TE=8.6/3.38, FOV 21×21cm.

The following experiments are carried out:

1) Test of the reconstruction quality as a function of the removed window size. We simulate two accelerated acquisitions with 32 and 16 ACS lines (effective acceleration factors of 2.37 and 2.67 respectively) and uniform acceleration factor $R = 3$. Large acceleration rate is considered to highlight the differences in reconstruction. A square window of size $N \times N$ is removed from the center of the ACS lines for estimation. N will range from 1 to 31 (for 32 ACS lines) and from 1 to 15 (for 16 ACS lines). The experiment is repeated for a round window of diameter N. For numerical comparison, two quality indexes are used: the Mean Squared Error (MSE) (13) and the Structural Similarity Index (SSIM) (14). The first index gives a measure for the global error in the image, while the second compares the structural similarities. For the latter, the closer to one, the better the reconstruction is. The comparison is done over the CMS in the **x**-space.

2) Validation of the assumption for the optimum size for N proposed in eq. [3]. We simulate acquisitions with 16, 24 and 32 ACS and acceleration rates of 2, 3 and 4. We will use the MSE of the reconstructed signal as a quality measure. To increase the number of experiments and to test low SNR data, Gaussian noise is added to each of the signals, so that

$$\max(\text{SNR}) = \frac{\max\{S_l(\mathbf{x})\}}{\sigma} = 25$$

3) Test of the reconstruction quality for a fixed window for different acceleration rates and number of ACS lines. The data is subsampled at three different rates, R=2, R=3 and R=4, and 32, 24 and 16 ACS lines are considered. The size of the removed window will be dynamically selected as a function of R and the number of lines accordingly to the results of the previous experiment. For comparison MSE and SSIM are used.

4) Finally, we will compare the proposed method with other GRAPPA improvements from literature: Fast Robust (FR) GRAPPA (8), High-pass GRAPPA (HP) and Non-linear (NL) GRAPPA (6). All the algorithms are similarly built in MATLAB and MSE and execution time are measured. As an illustration of the possibility of using the proposed method together with existing ones, we will merge it with FR-GRAPPA and HP-GRAPPA.

RESULTS

Results for the first experiment are collected in Table I (32 ACS) and Table II (16 ACS). $N = 0$ denotes the case in which no window is removed from the ACS, i.e., the standard GRAPPA. For the 32 ACS acquisition, note that, as N grows, the MSE

---

[1]`http://www.ece.tamu.edu/~jimji/pulsarweb/index.htm`

| | Data Set 1 | | Data Set 2 | | Data Set 3 | |
Window Size	MSE	SSIM	MSE	SSIM	MSE	SSIM
0	3.9150	0.8828	6.3934	0.7885	5.3948	0.7788
1	3.6389	0.8976	6.1485	0.7991	5.1335	0.7933
3	3.5539	0.9022	5.7116	0.8166	3.9796	0.8571
5	3.3378	0.9118	5.3058	0.8357	2.8824	0.9229
7	3.0320	0.9246	4.7674	0.8644	2.5899	0.9373
9	2.8090	0.9351	4.5686	0.8777	2.3631	0.9456
11	**2.7675**	0.9386	**4.4532**	0.8863	2.2439	0.9499
13	2.8485	0.9448	5.0665	0.8903	**2.2027**	**0.9527**
15	3.3027	**0.9478**	6.2879	**0.8939**	5.2342	0.9198

TABLE II. Reconstruction performance for different size N of the removed square window $\mathcal{C}_{\mathbf{k}}[N \times N]$ for the 3 Data Sets, acceleration factor $R = 3$ and 16 ACS lines.

| | | N for min{MSE} | | | | | | |
ACS	R	DS1	DS1+Noise	DS2	DS2+Noise	DS3	DS3+Noise	Average	Median
32	2	31	27	29	31	25	29	28.66	29
32	3	31	29	27	31	25	27	28.33	28
32	4	27	27	27	27	25	25	26.33	27
24	2	23	21	21	21	17	21	20.66	21
24	3	23	19	19	23	17	21	20.33	20
24	4	19	19	19	21	17	19	19	19
16	2	13	11	13	13	13	13	12.66	13
16	3	13	11	11	11	13	13	12	12
16	4	11	11	11	11	11	11	11	11

TABLE III. Optimal size N of the removed window $\mathcal{C}_{\mathbf{k}}$ as a function of the number of ACS lines and the acceleration factor R.

decreases and the SSIM index increases, showing both an improvement in the final quality of the reconstructed image. Note that the MSE reduces up to a 45% (3.5 to 1.9) for DS1 and almost to 50% for DS2. When the window size is too large, close to the number of ACS, we can also detect a slight degradation of the indexes, due to an excessive loss of data for estimation, but even then, there is a clear improvement when compared to the original GRAPPA method. In addition, we can see that there is not any particular advantage of using of a round window vs. a square one.

A similar behavior can be observed for the 16 ACS lines experiment. In this case, the degradation of the quality when the removal is excessive is much more clear, due to a smaller size of the estimation area and the smaller amount of data available for estimation. Nevertheless, it also shows a great reduction of the error when the central part of the **k**-space is removed. Note that the estimation with 16 ACS lines removing a 11×11 window is even better than a traditional 32 ACS acquisition. The proper choice of the samples used for estimation increases the accuracy of the reconstruction. The number of ACS lines can be reduced and even the acceleration rate can be increased, getting a higher final effective acceleration rate.

Results for the second experiment are collected in Table III. The optimal size for N is selected as

$$N_{\text{opt}} = \arg \min_{N}\{\text{MSE}\}.$$

The average and the median for each pair [ACS,R] are considered. The median results for the experiments are totally consistent with eq. [3]. However, there are particular cases in which the maximum lays in smaller sizes. The selected size will depend on several parameters like the acquisition modality and probably the SNR. Therefore, a calibration step may be necessary.

Results for the third experiment are collected in Table IV. FD-GRAPPA stands for Frequency Discriminated GRAPPA, the proposed method. The optimal window size in eq. [3] is used. N/A denotes the case in which the unsampled lines are simply padded with zeros (no reconstruction method is applied). In all the cases, the MSE improves when using FD. This is particularly significant for DS3 and $R = 4$, where the original GRAPPA shows an error larger than the non-reconstructed case. The error of the proposed method is about 5 times smaller than GRAPPA. For very high (and unrealistic) acceleration rates like $R = 4$, the first two data sets shows a better SSIM for the N/A case than the proposed method. However, note that even then FD is better than classical GRAPPA.

For the sake of illustration, some visual results for DS1 and DS3 are shown in Fig. 5. There is a clear improvement in the visual quality of the reconstructed data when FD is used. Note that even for high acceleration rates (R=4) FD-GRAPPA is able to recover images with an acceptable visual quality, when the traditional GRAPPA fails. Similar results can be seen in the doped ball phantom, for $R = 3$. We can appreciate a texture pattern inside the ball in the traditional GRAPPA reconstruction that does not appears in FD.

Finally, results for the comparative experiment are on Table V. For FR-GRAPPA a 10% outlier rejection is selected (the one that gives the best performance in the three data sets). For HP-GRAPPA optimal result have been found for $c = 10$ and $w = 2$.

SSIM									
Acceleration	2			3			4		
ACS	32	24	16	32	24	16	32	24	16
N/A	0.9321	0.9094	0.8747	0.9327	0.9086	0.8550	**0.8964**	**0.8964**	**0.8571**
GRAPPA	0.9625	0.9575	0.9484	0.9012	0.8938	0.8828	0.6280	0.6280	0.6094
FD-GRAPPA	**0.9807**	**0.9779**	**0.9744**	**0.9636**	**0.9556**	**0.9351**	0.8773	0.8773	0.8475
MSE									
Acceleration	2			3			4		
ACS	32	24	16	32	24	16	32	24	16
N/A	4.5615	5.9804	8.2481	5.1398	6.8181	10.0232	6.1890	6.1890	8.1462
GRAPPA	1.9727	2.1199	2.3793	3.5086	3.6729	3.9150	11.2902	11.2902	11.9503
FD-GRAPPA	**1.4448**	**1.5469**	**1.6598**	**2.0321**	**2.2776**	**2.8090**	**4.2099**	**4.2099**	**4.8756**

(a) Data set 1

SSIM									
Acceleration	2			3			4		
ACS	32	24	16	32	24	16	32	24	16
N/A	0.9031	0.8660	0.8262	0.9168	0.8849	0.8170	**0.8594**	**0.8594**	**0.8078**
GRAPPA	0.9212	0.9165	0.9091	0.8096	0.7997	0.7885	0.4883	0.4883	0.4746
FD-GRAPPA	**0.9557**	**0.9500**	**0.9402**	**0.9294**	**0.9118**	**0.8777**	0.7961	0.7961	0.7354
MSE									
Acceleration	2			3			4		
ACS	32	24	16	32	24	16	32	24	16
N/A	5.7886	8.2774	12.1783	6.2917	8.9411	14.3937	7.7442	7.7442	10.8953
GRAPPA	3.2484	3.3780	3.5769	5.8274	6.0765	6.3934	17.4195	17.4195	18.3490
FD-GRAPPA	**2.4234**	**2.6259**	**2.8980**	**3.2245**	**3.7497**	**4.5686**	**6.5033**	**6.5033**	**8.0746**

(b) Data set 2

SSIM									
Acceleration	2			3			4		
ACS	32	24	16	32	24	16	32	24	16
N/A	0.8782	0.8444	0.7943	0.8951	0.8746	0.7992	0.8259	0.8259	0.7764
GRAPPA	0.9149	0.9011	0.8790	0.8075	0.7932	0.7788	0.5142	0.5142	0.4960
FD-GRAPPA	**0.9711**	**0.9675**	**0.9642**	**0.9689**	**0.9639**	**0.9456**	**0.9074**	**0.9074**	**0.8844**
MSE									
Acceleration	2			3			4		
ACS	32	24	16	32	24	16	32	24	16
N/A	6.2345	7.7624	10.1849	7.2698	8.8445	11.6881	8.4905	8.4905	10.5451
GRAPPA	2.8984	3.1534	3.5413	4.8167	5.1035	5.3948	15.5504	15.5504	16.6166
FD-GRAPPA	**1.6568**	**1.7552**	**1.8529**	**1.7004**	**1.8479**	**2.3631**	**3.2237**	**3.2237**	**3.7835**

(c) Data set 3

TABLE IV. Results for the second experiment: the size of the window is dinamically chosen. (N/A stands for non parallel imaging Applied).

Again, the use of FD improves the MSE when compared with GRAPPA, but also note that the acquisition is accelerated, due to the reduction in the number of equations used to estimate the weights. The proposed method even improves FR-GRAPPA and HP-GRAPPA while being much faster than the former. When FD is used together with another optimization method, FD+FR and FD+HP, the MSE is even better and the execution time is reduced. Result of the NL-GRAPPA algorithm is, in all cases, slightly better that the proposed method. However, note that this improvement goes with a huge processing time when compared with FD-GRAPPA (23 minutes vs. 1 second).

CONCLUSIONS

The ACS lines commonly used to estimate the GRAPPA coefficients comprise high, medium, and also low frequency samples, meanwhile the lines to be retrieved by interpolation range from medium to high frequencies. As a result, the estimation of the interpolation weights becomes biased towards the high energy, low frequency spectrum. A simple elimination of the center samples of the ACS lines will highly improve the accuracy of the GRAPPA coefficients and therefore the final image reconstruction. At the same time, a reduction in the number of equations will accelerate the estimation. This simple method gives better results
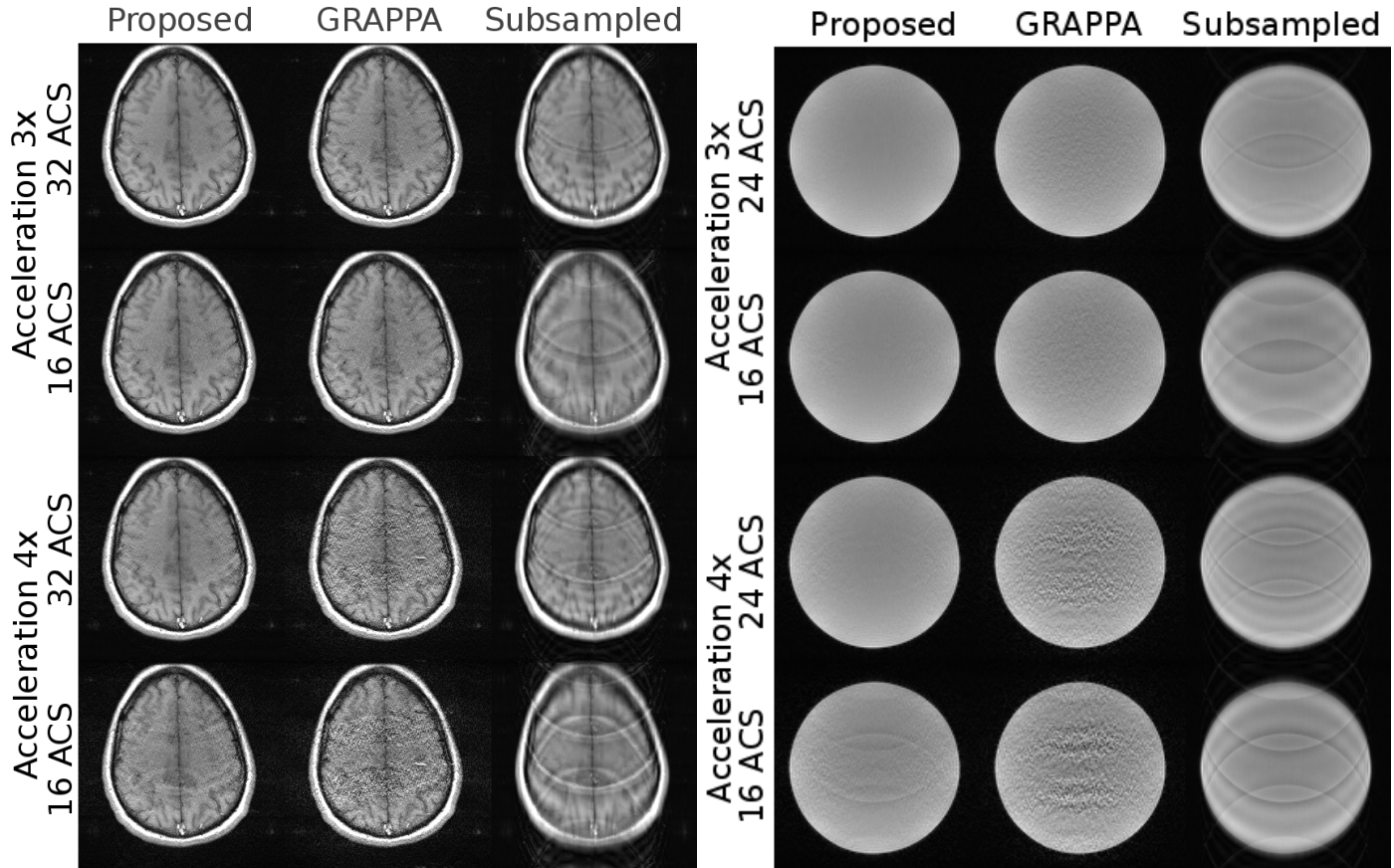
Figure 5. Reconstruction of subsampled MRI data from 8 coils using GRAPPA

	GRAPPA	FD	FR (10%)	FD+FR (10%)	HP	FD+HP	NL
Data set 1, 32 ACS $R = 3$							
MSE	3.5086	**1.9927**	2.1733	**1.8859**	2.0991	**1.9598**	**1.7347**
Time(s)	1.27	**1.24**	157.47	82.45	1.41	**1.25**	1379.2
Data set 2, 32 ACS $R = 3$							
MSE	5.8486	**3.1226**	3.3832	**2.9429**	3.3106	**3.0733**	**2.7222**
Time(s)	1.28	**1.25**	163.26	125.65	1.31	**1.26**	1401.3
Data set 3, 16 ACS $R = 3$							
	GRAPPA	FD	FR (10%)	FD+FR (5%)	HP	FD+HP	NL
MSE	5.5415	**2.2027**	3.1912	**2.1818**	2.7424	3.0742	**2.1818**
Time(s)	0.33	**0.28**	30.64	13.65	0.33	**0.29**	226.91

TABLE V. Comparison of different GRAPPA improvement algorithms

than traditional GRAPPA even with the half of the ACS lines. In addition, the improvement of the reconstruction quality makes it feasible using higher acceleration rates. The method is also compatible with other GRAPPA optimization techniques, such as outlier rejection, leading to further improvements in the final reconstruction. The simplicity of the method makes it suitable to be easily incorporated in commercial scanners.

REFERENCES

1. M. A. Griswold, P. M. Jakob, R. M. Heidemann, *et al.*, Generalized autocalibrating partially parallel acquisitions (GRAPPA), Magn. Reson. Med. 47 (6) (2002) 1202–1210.

2. S. Park, J. Park, Adaptive self-calibrating iterative GRAPPA reconstruction, Magn. Reson. Med. 67 (6) (2012) 1721–1729.
3. Z. Chen, J. Zhang, R. Yang, P. Kellman, L. A. Johnston, G. F. Egan, IIR GRAPPA for parallel MR image reconstruction, Magn. Reson. Med. 63 (2) (2010) 502–509.
4. C. Wu, W. Hu, R. Kan, J. Yu, X. Sun, An improved GRAPPA image reconstruction algorithm for parallel MRI, in: Control and Decision Conference (CCDC), 2011 Chinese, 2011, pp. 4096 –4100.
5. F. Huang, Y. Li, S. Vijayakumar, S. Hertel, G. R. Duensing, High-pass GRAPPA: An image support reduction technique for improved partially parallel imaging, Magn. Reson. Med. 59 (3) (2008) 642–649.
6. Y. Chang, D. Liang, L. Ying, Nonlinear GRAPPA: A kernel approach to parallel MRI reconstruction, Magn. Reson. Med. 68 (3) (2012) 730–740.
7. H. Wang, D. Liang, K. F. King, G. Nagarsekar, Y. Chang, L. Ying, Improving GRAPPA using cross-sampled autocalibration data, Magn. Reson. Med. 67 (4) (2012) 1042–1053.
8. D. Huo, D. Wilson, Robust GRAPPA reconstruction and its evaluation with the perceptual difference model, J. Magn. Reson. 27 (6) (2008) 1412–20.
9. W. S. Hoge, D. H. Brooks, B. Madore, W. E. Kyriakos, A tour of accelerated parallel MR imaging from a linear systems perspective, Concepts Magn Reson Part A 27A (1) (2005) 17–37.
10. M. Blaimer, F. Breuer, M. Mueller, R. Heidemann, M. Griswold, P. Jakob, SMASH, SENSE, PILS, GRAPPA: how to choose the optimal method, Top Magn Reson Imaging 15 (4) (2004) 223–236.
11. J. S. Lim, Two Dimensional Signal and Image Processing, Prentice Hall, Englewood Cliffs, NJ, 1990.
12. J. X. Ji, J. B. Son, S. D. Rane, PULSAR: A matlab toolbox for parallel magnetic resonance imaging using array coils and multiple channel receivers, Concepts in Magnetic Resonance Part B: Magnetic Resonance Engineering 31B (1) (2007) 24–36.
13. A. Eskicioglu, P. Fisher, Image quality measures and their performance, IEEE Trans. Comm. 43 (12) (1995) 2959–2965.
14. Z. Wang, A. C. Bovik, H. R. Sheikh, E. P. Simoncelli, Image quality assessment: from error visibility to structural similarity, IEEE Trans. Image Proccess. 13 (4) (2004) 600–612.